

This is an Open Access document downloaded from ORCA, Cardiff University's institutional repository:<https://orca.cardiff.ac.uk/id/eprint/109839/>

This is the author's version of a work that was submitted to / accepted for publication.

Citation for final published version:

Liang, Weihui, Huang, Jianxiang, Jones, Phil , Wang, Qun and Hang, Jian 2018. A zonal model for assessing street canyon air temperature of high-density cities. *Building and Environment* 132 , pp. 160-169. 10.1016/j.buildenv.2018.01.035

Publishers page: <http://dx.doi.org/10.1016/j.buildenv.2018.01.035>

Please note:

Changes made as a result of publishing processes such as copy-editing, formatting and page numbers may not be reflected in this version. For the definitive version of this publication, please refer to the published source. You are advised to consult the publisher's version if you wish to cite this paper.

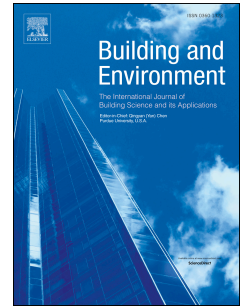
This version is being made available in accordance with publisher policies. See <http://orca.cf.ac.uk/policies.html> for usage policies. Copyright and moral rights for publications made available in ORCA are retained by the copyright holders.



Accepted Manuscript

A zonal model for assessing street canyon air temperature of high-density cities

Weihui Liang, Jianxiang Huang, Phil Jones, Qun Wang, Jian Hang



PII: S0360-1323(18)30047-7

DOI: [10.1016/j.buildenv.2018.01.035](https://doi.org/10.1016/j.buildenv.2018.01.035)

Reference: BAE 5271

To appear in: *Building and Environment*

Received Date: 24 October 2017

Revised Date: 9 January 2018

Accepted Date: 25 January 2018

Please cite this article as: Liang W, Huang J, Jones P, Wang Q, Hang J, A zonal model for assessing street canyon air temperature of high-density cities, *Building and Environment* (2018), doi: 10.1016/j.buildenv.2018.01.035.

This is a PDF file of an unedited manuscript that has been accepted for publication. As a service to our customers we are providing this early version of the manuscript. The manuscript will undergo copyediting, typesetting, and review of the resulting proof before it is published in its final form. Please note that during the production process errors may be discovered which could affect the content, and all legal disclaimers that apply to the journal pertain.

1 *Manuscript for **Building and Environment***

2 A Zonal Model for Assessing Street Canyon Air Temperature
3 of High-Density Cities

4 Weihui Liang^{a,b}, Jianxiang Huang^{a,c*}, Phil Jones^d, Qun Wang^e, Jian Hang^f

5 ^a8/F Knowles Building, Department of Urban Planning and Design, the University of
6 Hong Kong, Pokfulam Road, Hong Kong, China

7 ^bSchool of Architecture and Urban Planning, Nanjing University, Nanjing, China

8 ^cShenzhen Institute of Research and Innovation, The University of Hong Kong

9 ^dWelsh School of Architecture, Cardiff University, King Edward VII Avenue, Cardiff
10 CF10 3NB, UK

11 ^eDepartment of Mechanical Engineering, The University of Hong Kong, Pokfulam
12 Road, Hong Kong Special Administrative Region

13 ^fSchool of Atmospheric Sciences, Sun Yat-Sen University, Guangzhou, P. R. China

14 *Corresponding author:

15 Dr. Jianxiang Huang

16 8/F Knowles Building, Department of Urban Planning and Design, the University of
17 Hong Kong, Pokfulam Road, Hong Kong, China

18 Tel: +852 2219 4991

19 Fax: +852 2559 0468

20 Email: jxhuang@hku.hk

21 **Abstract**

22 The microclimate of a high-density city affects building energy consumption and
23 thermal comfort. Despite the practical needs in building design and urban planning to
24 predict conditions inside street canyons, literature is sparse for physics-based models
25 that can support early stage design. Existing tools such as the Computational Fluid
26 Dynamics (CFD) method is computationally expensive and cannot easily be coupled
27 with other simulation models to account for solar heat gains at urban surfaces and
28 anthropogenic heat from traffic and building HVAC systems. This paper describes a
29 zonal model developed to assess airflow and air temperature in street canyons in
30 high-density cities. The model takes into account 3D urban geometries, external wind,
31 buoyancy, convective heat transfers from urban surfaces; it can simulate zonal air
32 temperature, pressure, and airflow patterns by interactively solving mass, pressure and
33 energy balance equations. The model was evaluated using field measurement on a
34 'mock-up' site consisted of movable concrete bins mimicking buildings and street
35 canyons in high-density cities. Experiments were conducted on 3 alternative street
36 layouts of various height-to-width aspect ratios: moderate ($H/W=1$), dense ($H/W=2$),
37 and high-density ($H/W=3$). Agreements between predicted and measured air
38 temperatures were satisfactory across 3 layouts ($R^2>0.964$). Temperature differences
39 between simulated and measured results were largely within 1 K. The model can
40 provide a reliable and quick assessment of the impact of street canyons on urban heat

41 island (UHI) in high-density cities. The next step is to couple this model with building
42 energy models.

43

44 **Keywords:** Zonal Model; Urban Heat Island; Street Canyon Air Temperature;
45 Microclimate; Mock-Up Site

46 **1. Introduction**

47 The urban microclimate inside street canyons can have a major effect on the thermal
48 comfort of pedestrians as well as building energy performance [1] [2]. Previous work
49 has identified the need to assess urban microclimate in relation to the rapid growth of
50 the urban population worldwide [3]. The growing urbanization drives the expansion
51 of the urban area, creating more high-rise buildings, high-density cities and
52 mega-cities [4] [5]. Building and urban design influence the urban microclimate, and
53 human anthropogenic heat generation generally intensifies the differences between
54 urban and rural microclimates [6]. The urban heat island (UHI) which is characterized
55 by higher temperatures in urban areas than in rural areas is widely reported [6–8].
56 However, in most of the current building energy design processes, the microclimate
57 around a building is not taken into consideration, and the energy demand is predicted
58 using the meteorological data obtained from a suburban or rural weather station (i.e. a
59 nearby airport) [9]. This simplification can generally lead to an overestimation of the
60 annual heating load and underestimation of the cooling load compared to the situation
61 with consideration of the urban microclimate around the building [10]. Thus, the
62 studies of the urban microclimate in street canyons are significant for the optimization
63 of urban design and building energy simulation.

64 Research literature on urban microclimate indicates experimental and numerical
65 activities. The experimental approach can provide direct measurement data, showing
66 the effects of different influencing factors such as the street layout and meteorological
67 conditions etc. Santamouris et al. [11] measured the airflow and temperature in a deep
68 pedestrian canyon over a week and found that there were spatial and temporal
69 variations of the surface and air temperatures inside the canyon. Johansson [12] found
70 that the average air temperature in the deep street canyon was 6 K lower than the
71 shallow one and thus it was more comfortable in summer. Karra et al. [13] conducted

72 a field and laboratory study and found that the flow field showed a clear sensitivity to
73 the local geometry. However, the experimental methods are expensive and only
74 limited cases can be studied. Moreover, due to the limited number of the instruments,
75 the measurement data is discrete in time and space. Thus, numerical methods have
76 been developed to assess the microclimate in street canyons. The computational fluid
77 dynamics (CFD) model is the most common numerical simulation approach which
78 can simulate the detailed airflow and temperature distribution of the urban domain.
79 Bruse and Fler [14] introduced a model named ENVI-met, in which a
80 non-hydrostatic microclimate model designed to simulate the surface-plane-air
81 interactions in an urban environment. Chatzidimitriou and Axarli [15] simulated the
82 effects of geometry on microclimate and comfort in the street canons by ENVI-met.
83 Oguro et al. [16] established a wind environment database for the assessment system
84 CASBEE-HI (Comprehensive Assessment System for Building Environmental
85 Efficiency on Heat Island Relaxation) by CFD simulation. Yang and Li [17] used a
86 three-dimensional urban surface energy balance model and studied the impact of
87 urban geometry on average urban albedo and street surface temperature. The outdoor
88 thermal environment has also been analyzed using CFD models[18,19], while the
89 buoyancy effect of solar radiation is complex and cannot be easily accounted for in
90 the CFD simulation of external spaces [20], although recent attempts were made
91 coupling CFD and building energy models together [21]. Jeanjean et al. [22] analyzed
92 the combined influence of building morphology and trees on air pollutant
93 concentration in a neighbourhood by CFD. Wen et al. [23] performed CFD simulation
94 and studied the flow behavior of the aeration around buildings. Many other studies
95 used the CFD model to analyze the microclimate in the street canyons could be found
96 [24–26]. The CFD method, despite many merits, are confronted with difficulties when
97 applied to large districts and complex urban configurations [27] and it is
98 computationally expansive, making it practically difficult to support building design

99 and urban planning practices in which reliable and quick assessment are needed at
100 early stages.

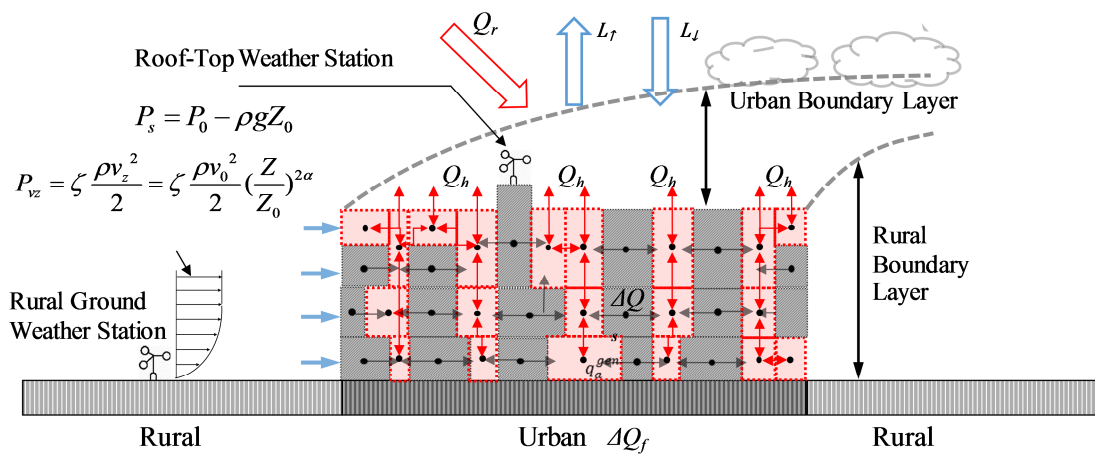
101 In light of many practical limitations of CFD models, other alternatives methods were
102 developed to assess airflow or temperature in street canyons. De La Flor and
103 Domínguez [28] presented a numerical urban canyon model to assess the modification
104 of climatic variables in an urban context. Musy et al. [29] proposed a zonal model to
105 assess the indoor air temperature and flow. This method was also meaningful to the
106 model development of outdoor microclimate simulation in street canyons. Bozonnet
107 et al. [30] developed an empirical model to assess the airflow within the street canyon.
108 Djedjig et al. [31] proposed a hygrothermal model of green walls and coupled it with
109 the model of mass flows in street canyons to assess the thermal impact of green walls
110 on buildings as well as the surrounding microclimate. Masson [32] presented an urban
111 surface scheme for atmospheric mesoscale models. Yao et al. [20] developed a nodal
112 network method to model the urban microclimates and validated it against field
113 measurement data on the campus of Chongqing University. However, the vertical air
114 temperature and flow profiles could not be predicted with this method.

115 This study describes the development of a zonal model to simulate the dynamic urban
116 microclimate of street canyons in high-density cities. The horizontal and vertical
117 temperature distributions across the simulation domain, air exchange between zones,
118 can be simulated. Mathematical models and boundary conditions of the zonal model
119 are described. Scale-model outdoor field experiments have been carried out and
120 compared with the simulation results. The resulting zonal model is able to predict the
121 time varying air temperature in street canyons quickly with acceptable accuracy,
122 which has promising applications in the stages of urban and building design.

123 **2. Method of the mathematic model**

124 The basic idea of zonal modelling is to divide the street canyons into multiple zones

125 connected with each other. The air in each zone is assumed to be well-mixed with a
 126 uniform air temperature. The vertical division of zones is used to account for the
 127 vertical distribution of temperature within deep street canyons. Fig. 1 illustrates a
 128 typical zonal division for the outdoor environment. The height in the same level of the
 129 zones is set to be identical. Dimensions and divisions of the zones describe the
 130 building and canyon geometries and layouts of the domain. Pressure, temperature and
 131 air density in each zone of the domain follow the ideal gas law. The zonal method is
 132 based on mass and heat balances for the macroscopic volumes.



133

134 **Fig. 1** Schematic depiction of the zonal urban microclimate model.

135

136 2.1 Mass and heat balances

137 2.1.1 Mass balance in the network

138 Airflow takes place across the inter-connected zones, with mass variations due to air
 139 density differences assumed negligible in an urban environment. Thus, the zonal mass
 140 balance equation can be expressed as:

141

$$\sum_{j=1}^{j=N} (m_{ij} - m_{ji}) = M_{si} \quad (1)$$

142 where m_{ij} and m_{ji} are the mass flow rate from zone i to zone j and zone j to zone i
 143 respectively (kg/s), and both are defined as “positive” variables; M_{si} is the rate of
 144 mass accumulation in zone i (kg/s), while N is the number of the zone.

145 2.1.2 Heat balance in the network

146 Heat transfer occurs between zones due to mass exchanges or between air and
 147 surfaces, i.e. building walls, roofs and the ground. The zonal heat balance equation is
 148 expressed as:

$$149 \quad \rho_i V_i c_p \frac{dT_i}{dt} = \sum_{j=1}^{j=N} (m_{ji} c_p T_j - m_{ij} c_p T_i) + \sum_{k=1}^{k=M} h_k A_k (T_{surf} - T_i) + \sum_{a=1}^{a=S} Q_{si} \quad (2)$$

150 where the term in the left hand is the heat change of the air, the first term in the right
 151 hand represents the heat exchange due to mass flow exchange, the second term in the
 152 right hand is the convective heat flux, the third term is power of heat generation from
 153 anthropogenic source. ρ_i is the zonal air density (kg/m³); V_i is the zonal volume
 154 (m³); c_p is the specific heat capacity of the air (J/kg.K); T_i and T_j are the air
 155 temperature of zone i and zone j (K); h_k is the convective heat transfer coefficient
 156 between the surface and air (W/m².K); A_k is the area of the surface (m²); T_{surf} is the
 157 surface temperature (K); Q_{si} is the power of heat generation from anthropogenic
 158 source within zone i (W), i.e. traffic, air conditioning (AC) units, or cooking. The
 159 surface temperature T_{surf} can be obtained by an energy balance equation on the surface
 160 or measured onsite directly.

161 2.2 Pressure and airflow balances

162 The airflow between zones is driven by pressure and density differences. Flows are
 163 calculated for 1) horizontal and 2) vertical opening accordingly. The inclined opening
 164 could be equivalent to a horizontal opening and a vertical opening with different areas

165 according to the projection.

166 2.2.1 Airflow model at horizontal opening

167 For horizontal openings, the hydrostatic variation of pressure between the horizontal
168 connected two zones (ΔP_{ji}) is expressed below [22] [24] [25]:

$$169 \quad \Delta P_{ji} = P_j - P_i - \frac{1}{2} g(\rho_i h_i + \rho_j h_j) \quad (3)$$

170 where P_j , ρ_j and h_j are the pressure, air density and overall height of the upper zone j .
171 P_i , ρ_i and h_i are the pressure, air density and overall height of the bottom zone i . g is
172 the gravitational acceleration (m/s^2).

173 Thus mass flow rate across the horizontal opening can be expressed as:

$$174 \quad m_{ji} = \mu A \sqrt{2\rho_j \Delta P_{ji}}, \quad m_{ij} = 0, \quad \text{if } \Delta P_{ji} > 0 \quad (4)$$

$$175 \quad m_{ij} = \mu A \sqrt{2\rho_i |\Delta P_{ji}|}, \quad m_{ji} = 0, \quad \text{if } \Delta P_{ji} < 0 \quad (5)$$

176 where μ is the discharge coefficient of the opening; A is the area of the opening (m^2).
177 The discharge coefficient is depended on the opening Reynold number, wind
178 incidence angle and direction of air flow, size and shape of the opening [35,36].

179 2.2.2 Airflow model at vertical opening

180 For vertical openings, when there is temperature difference between zones, this
181 temperature difference will result in an air density difference, leading to a positive
182 pressure difference at the top of the opening and a negative pressure difference at the
183 bottom (or vice versa) [37]. Two-way airflow may occur according to the position of
184 the neutral level. At the neutral level, the air velocity is zero, which can be determined
185 according to the following equation.

186

$$Z_n = \frac{\Delta P}{(\rho_i - \rho_j)g} \quad (6)$$

187 where Z_n is the neutral level (m); ΔP is the pressure difference between zones (Pa).

188 The airflow model may vary in different conditions, according to the position of the

189 neutral level, therefore the airflow rate is categorized into the following situations.

190 (1) When $0 < Z_n < h$, the neutral level is within the opening. Two-way airflow

191 occurs at the vertical opening, which can be calculated by:

192

$$m_{ij} = \frac{2}{3} \mu W \sqrt{2g\rho_i |\rho_i - \rho_j|} (h - Z_n)^{\frac{3}{2}} \quad (7)$$

193

$$m_{ji} = \frac{2}{3} \mu W \sqrt{2g\rho_j |\rho_i - \rho_j|} (Z_n)^{\frac{3}{2}} \quad (8)$$

194 (2) When $Z_n \leq 0$, the neutral level is below the opening. The airflow is195 unidirectional and flows from zone i to zone j , which can be calculated by:

196

$$m_{ij} = \frac{2}{3} \mu W \sqrt{2g\rho_i |\rho_i - \rho_j|} \left[(h - Z_n)^{\frac{3}{2}} - (-Z_n)^{\frac{3}{2}} \right] \quad (9)$$

197

$$m_{ji} = 0 \quad (10)$$

198 (3) When $Z_n \geq h$, the neutral level is above the opening. Air flows from zone j to199 zone i , which can be calculated by:

200

$$m_{ij} = 0 \quad (11)$$

201

$$m_{ji} = \frac{2}{3} \mu W \sqrt{2g\rho_j |\rho_i - \rho_j|} \left[(Z_n)^{\frac{3}{2}} - (Z_n - h)^{\frac{3}{2}} \right] \quad (12)$$

202

203

where h is the overall height of the vertical opening (m); W is the width of the opening (m).

204 2.3 Boundary conditions

205 To solve the above mass and heat balance equations, the boundary conditions of the
206 model need to be provided or calculated, which include the wind, temperature and
207 pressure boundary conditions. There are five zones connected to the simulation
208 domain from the adjacent surroundings, which, for example, can represent the
209 boundary zones in the north, south, east, west directions and the upper boundary zone.

210 2.3.1 Wind boundary condition

211 The wind direction and speed will affect the wind pressure around the simulation
212 domain. The wind velocity in the rural boundary is prescribed by a power law
213 distribution, which is widely used in horizontal wind speed estimation[38–41]:

$$214 \quad v_z = v_0 \left(\frac{Z}{Z_0} \right)^\alpha \quad (13)$$

215 where v_z is the reference wind speed at height Z (m/s); v_0 is the wind speed measured
216 at the weather station (m/s); Z_0 is the height of the weather station (m). α is an
217 empirical constant depending on atmospheric condition, flow stabilities and surface
218 configurations.

219 2.3.2 Temperature boundary condition

220 The air temperature of the boundary zone influences the heat transfer between the
221 boundary and the simulation domain induced by the airflow, while surface
222 temperatures within the domain affect the heat transfer from the surfaces to the
223 specific zones. Thus, both air temperatures of the boundary zones and surface
224 temperatures of the exterior building envelopes, and the exterior ground temperatures
225 need to be provided. Air temperature of the boundaries zones, such as north, south,
226 west, east, and upper zones of the simulated domain, are assumed to be the same as
227 that at the local weather station. The surface temperatures of the buildings and ground

228 can either be calculated by a building energy and surface temperature models or
 229 measured onsite.

230 2.3.3 Pressure boundary condition

231 The static air pressure (P_s) at a given height Z can be inferred from a local weather
 232 station after adjusting for the stack effect due to gravity:

$$233 \quad P_s = P_0 - \rho g(Z - Z_0) \quad (14)$$

234 where P_0 is the measured barometric pressure at the operational weather station (Pa)
 235 and ρ is the density of the air (kg/m^3).

236 The wind pressure at the boundary surfaces of the simulated domain can be calculated
 237 according to the wind profile. The main differences between east, west, south and
 238 north surrounding zones are the values of the wind pressure coefficient ζ , which varies
 239 according to the wind direction. Thus, wind pressure (P_{vz}) at the boundary surfaces
 240 can be calculated by the following equation:

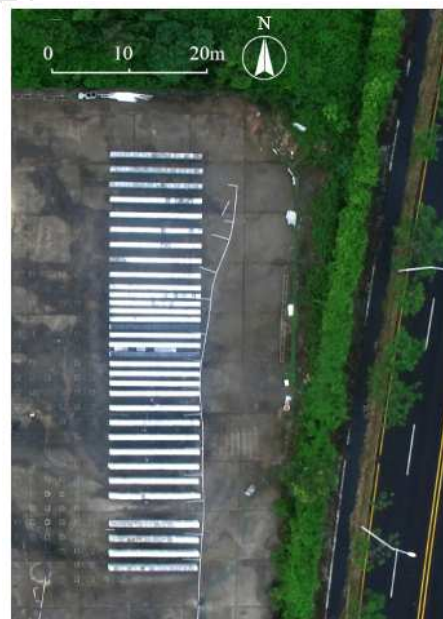
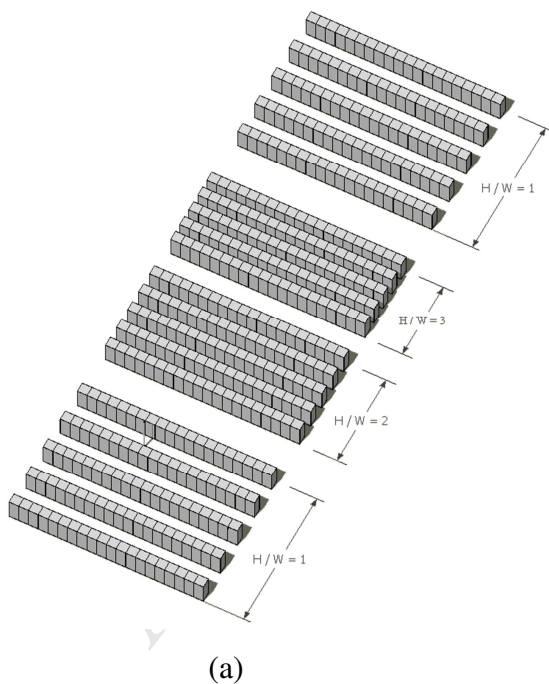
$$241 \quad P_{vz} = \zeta \frac{\rho v_z^2}{2} = \zeta \frac{\rho v_0^2}{2} \left(\frac{Z}{Z_0}\right)^{2\alpha} \quad (15)$$

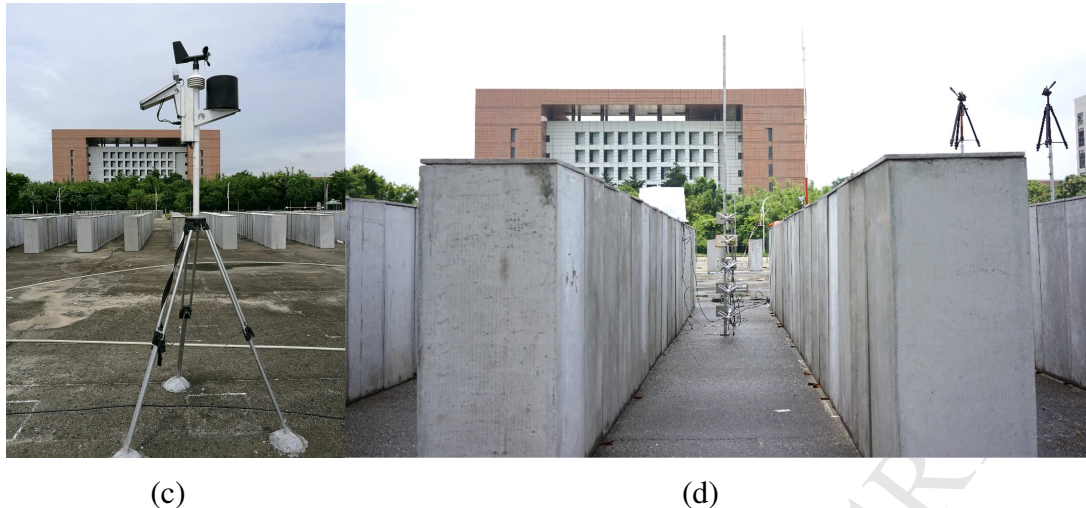
242 3. Model evaluation

243 3.1 Experimental setup

244 In order to evaluate the performance of the zonal model, scale-model outdoor field
 245 experiments were conducted in a mock-up site of Sun Yat-sen university campus in
 246 suburb region of Guangzhou, China ($23^\circ 4' \text{ N}$, $113^\circ 23' \text{ E}$). Fig. 2 shows the plan of the
 247 mock-up site. The mock-up street canyons were built with hollow concrete bins of 0.5
 248 m \times 0.5 m \times 1.2 m (width \times length \times height) with the wall thickness of 1.5 cm.
 249 During the experiment, a total number of 620 concrete bins were aligned in parallel
 250 rows along the east-west direction. Each row has 20 concrete bins numbered 1 to 20

251 starting from the east to west. The space in the mock-up street canyons could be
252 subdivide as 20 zones in accordance with the number of the concrete bins. Zone No.
253 12 was used as the target zone to validate the accuracy of the model. The widths of
254 the “street canyons” were made to 1.2 m, 0.6 m, and 0.4 m, which result in aspect
255 ratios (H/W) of 1, 2 and 3, respectively. The effect of the depth of the street canyon on
256 the microclimate around the buildings can be studied. These are simplified cases
257 compared to the actual street canyons in city. The advantages of carrying out a field
258 experiment on the mock-up site are that it allows reliable measurement of air
259 temperature, surface temperatures of the ground, wall and the roof, whereas in a real
260 city these variables cannot be easily measured and it is almost impossible to account
261 for anthropogenic heat emissions from traffic and other activities accurately.
262 Simulations have been compared with the measurement data, which were obtained in
263 the experiment conducted on 19–21 July 2016.





266
267
268

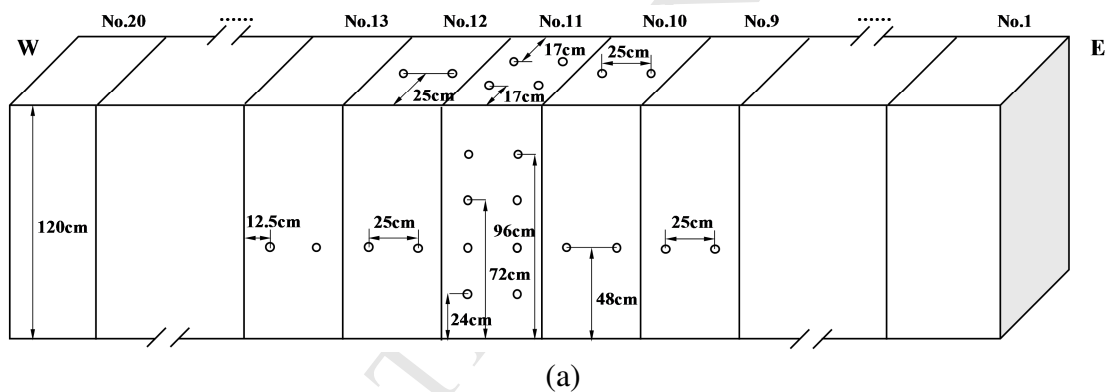
269 **Fig. 2** The experiment site. (a) Schematic illustration of the plan of the mock-up street
270 canyons with aspect ratios of moderate ($H/W=1$), dense ($H/W=2$), and high-density
271 ($H/W=3$), (b) Aerial photo of the mock-up site taken on 18 July 2016, (c) & (d)
272 Horizontal photos of the mock-up site taken on 18 July 2016

273

274 Measurements were conducted simultaneously and the locations of all the instruments
275 were the same for the three different aspect ratio scenarios. Air temperatures were
276 measured by iButton (DS 1922L) with shielding at the interval of 1 min. Two of them
277 were placed in the center of zone No. 12 at the height of 0.1 m and 0.6 m to measure
278 the air temperature in the mock-up street canyon. Another was placed at the height of
279 1.3 m to measure the air temperature above the canyons. The measurement range and
280 error of this instrument were -40 to 85 °C and ± 0.5 °C. Thermocouples were mounted
281 on the vertical walls, the ground and roof surfaces to measure the time-varying
282 surface temperatures. These surface temperature data were recorded continuously by
283 Agilent 34972A data loggers at intervals of 3 seconds. Due to limited numbers of
284 available equipment, only the surface temperatures of concrete bins No. 9–13 were
285 measured. Thus, surface temperatures of concrete No. 12 and other concretes near it
286 were measured in detail, which could assure the accuracy of the boundary conditions

287 of the target zone No. 12. Surface temperatures of concretes No. 1–8 and No. 14–20
 288 were assumed to be the same as that of concretes No. 9 and No. 13, respectively.
 289 Several lines of thermocouples were placed along the “wall” and “roof” surfaces to
 290 measure the temperature gradation as they were shown in Fig. 3(b)

291 **Fig. 3.** The positions of the thermocouples in the opposite “wall” and “roof” surfaces
 292 of the mock-up street canyon were the same. Five thermocouples were placed evenly at
 293 the central line of the ground surface of zone No. 12 at the north-south direction. To
 294 double-check surface temperature measurement from thermocouples, an infrared
 295 camera (FLIR P635) was used to take thermal imagery of the mock-up site on a
 296 regular basis. Comparison of the surface temperature measurement results between
 297 these two methods has been illustrated in Fig. S1 of the supporting information.





(b)

300

301

302 **Fig. 3** Instrument layout in the mock-up street canyon. (a) Illustration of the locations
 303 of the instruments (the “○” represents the thermocouples), (b) Photo of the sensors

304

305

306

307

308

309

310

311

312

313

314

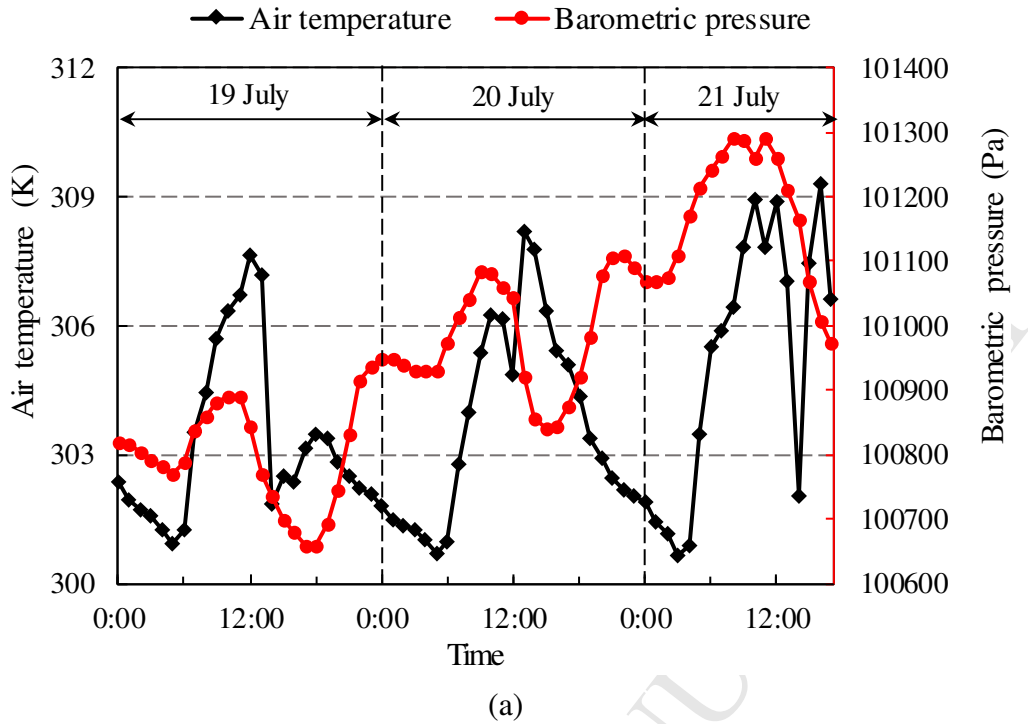
315

A weather station (RainWise PortLog) was used to measure the local air temperature, barometric pressure, solar radiation, rainfall, wind direction and speed, which could serve as the input boundary conditions for the modelling. It was located at the central of the experiment site at north-south direction. The distance between the west edge of the mock-up street canyons to the anemometer was 15 m. The monitoring time interval was set to 1 min. The sensors of the weather station were located at a height of 2.4 m above the ground. Theurer [41] concluded that for interrupted rows and row like buildings, the α value in equation 13 is recommended to be 0.36 and 0.44, respectively. The α was assumed to be 0.4 for the mock-up site in this study. Consequently, with the wind speed and height of the weather station are given, the vertical profile of the wind speed at different height could be calculated and thus the wind boundary condition could be obtained.

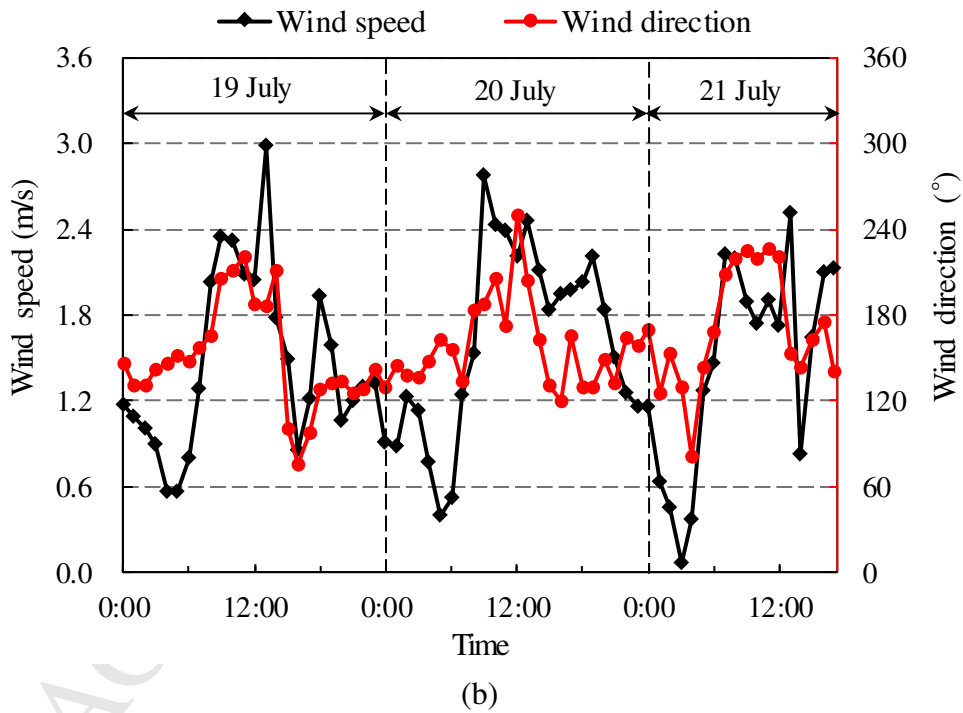
316 3.2 Measurement results

317 The hourly average local air temperature and barometric pressure are presented in Fig.
318 4(a). The air temperature ranged between 300–310 K (27–37 °C) during the
319 measurement period. Air temperatures at 14:00, 19 and 21 July decreased noticeably
320 due to the sudden showers at the period of 13:49–14:02, 19 July and 13:52–14:04, 21
321 July recorded by the local weather station. As the water absorbed by the concrete bins
322 could not be accurately estimated when it was raining, nor the amount of moisture
323 evaporating from the surfaces after the rain, the heat exchange at the concrete surfaces
324 due to this factor could not be well considered. Thus the effect of rain was not
325 considered in our simulation. Consequently, the simulated temperatures supposed to
326 be higher than the measured data at the rainy hours (13:00-14:00) and several hours
327 after (14:00-17:00).

328 The hourly average wind speed and direction are shown in Fig. 4(b). Wind from the
329 north direction corresponds to 0 ° in the figure. Recorded wind direction ranged from
330 76° to 250°, allowing assessment of conditions in which wind are parallel, transverse
331 or oblique to the street canyon. The actual wind speed and direction vary over time.
332 To simplify, hourly average wind direction and speed were used as the input boundary
333 conditions of the model to calculate the wind pressure around the mock-up street
334 canyons. The wind speed varied between 0.07 to 3.0 m/s and the wind direction
335 varied between 76 to 250 ° during the experiment.



336
337



338
339

340 **Fig. 4** Boundary conditions measured by the local weather station during the
341 measurement. (a) Air temperature and barometric pressure, (b) Wind speed and
342 direction (degrees from north)

343

344 Surface temperatures for different aspect ratios are presented in S2 and Fig. S2 of the
345 Supporting Information. Air temperatures at the mock-up street canyons are presented
346 in Fig. S3 of the Supporting Information. There were slight differences among
347 different scenarios.

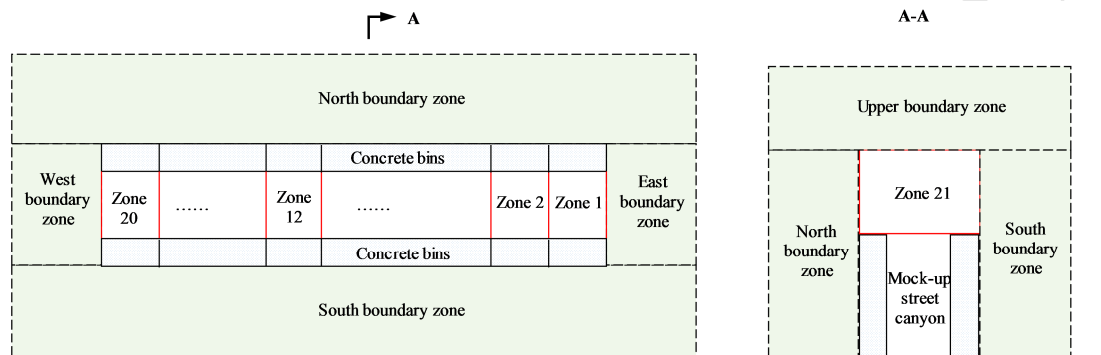
348 **3.3 Computer simulation**

349 The “street canyons” of the mock-up site were digitalized as inputs for the zonal
350 model. The linear space of the “street canyon” was segmented into 20 zones of equal
351 size, numbered 1 to 20 starting from east to west. Zone No. 21 was added on the top
352 of the street canyon and two rows of concrete bins. The height of this upper zone was
353 assumed to be 1.2 m and the length was 10 m. This could consider the heating or
354 cooling effects of the roof to the upper zone of the canyons. 21 zones of the
355 simulation domain, five boundary zones, namely the east, west, north, south and
356 upper boundary zones were included in the simulation. Fig. 5 shows the division of
357 the zones for the mock-up street canyon.

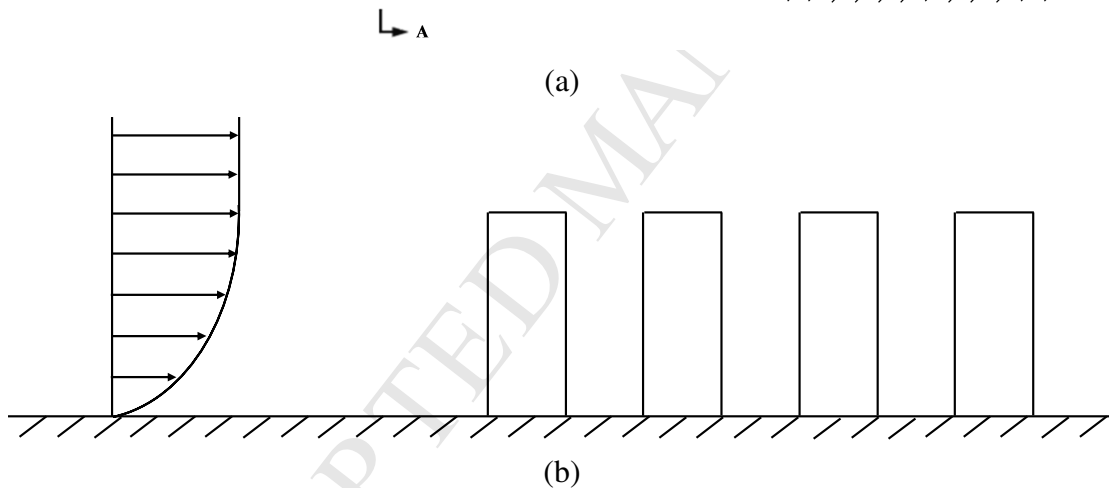
358 Generally speaking, the discharge coefficients μ in the equations for sharp-edged
359 openings are in the range of 0.6-0.65 [35,42,43]. In our case, we have a continuous
360 street canyon which is manually divided into zones. There are no valves nor
361 obstructions other than the canyon walls, thus the value is supposed to be larger. A
362 value of 1 was adopted in our simulation. Sensitivity analysis of discharge coefficients
363 on the simulation results were also included in the Supporting Information. The air
364 temperatures in the mock-up street canyon are not sensitive to the discharge
365 coefficient according to the results.

366 By inputting the surface temperatures of each zone and the measurement data of the
367 local weather station, together with the airflow model, heat and mass balance
368 equations in the zones, air temperature in each zone and airflow rates between zones
369 were simulated. The simulation results for zone No. 12 were compared with the

370 measured air temperature data. The calculation was executed using Python
 371 programming language. For condition in each hour, the calculation took less than 10
 372 seconds to reach convergence, in which the pressure, temperature and air flow
 373 residuals are less than 0.01 Pa, 0.0001 K and 0.06 kg/s respectively. Fig. 6 shows the
 374 convergence conditions of pressure, temperature and air flow at a typical hour.



375
 376



377
 378
 379
 380
 381

Fig. 5 (a) Division of zones for the mock-up street canyon; (b) Wind vertical profile of the study site ($\alpha = 0.4$)

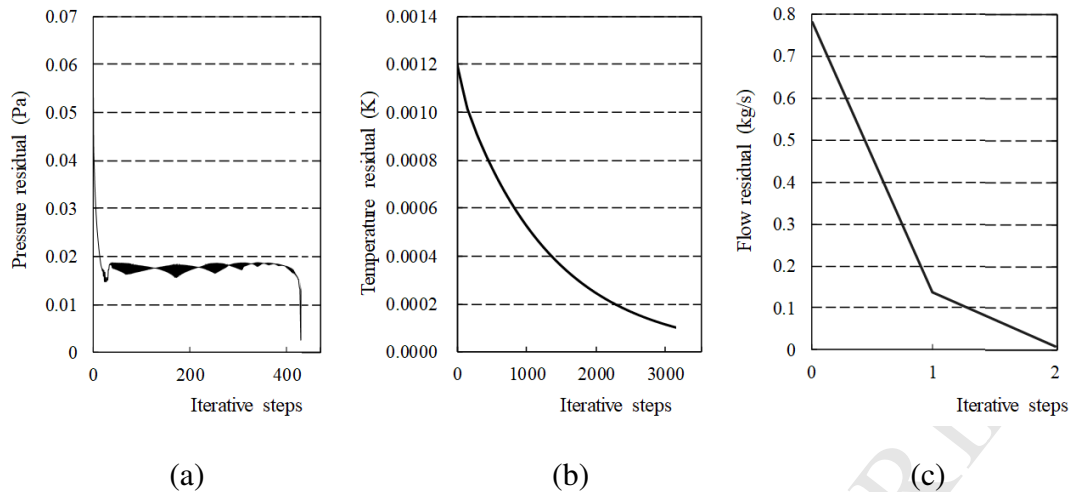
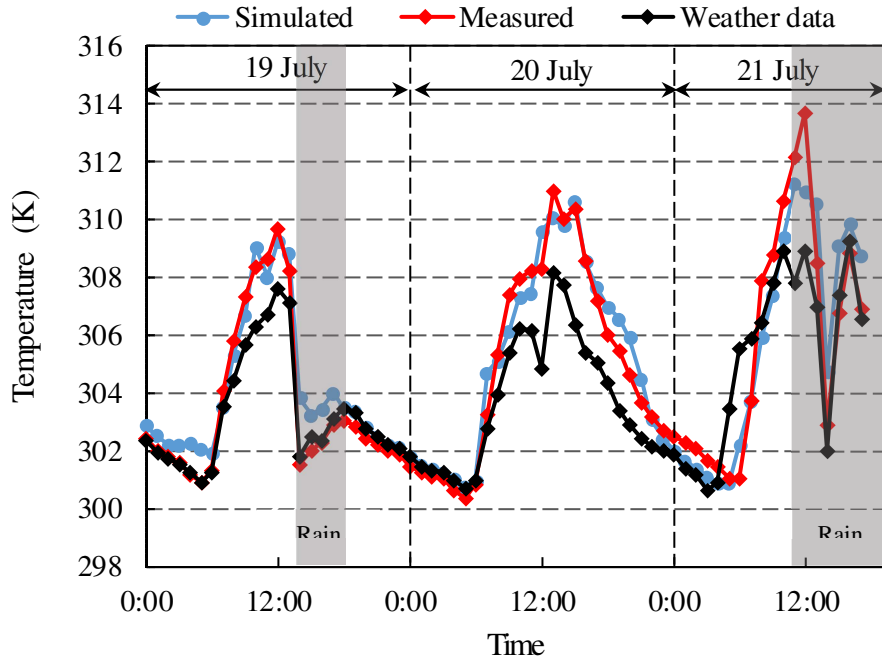


Fig. 6 Convergence of pressure, temperature and air flow at a typical hour. (a) Pressure residual (Pa), (b) Temperature residual ($^{\circ}\text{C}$), (a) Airflow residual (kg/s)

382

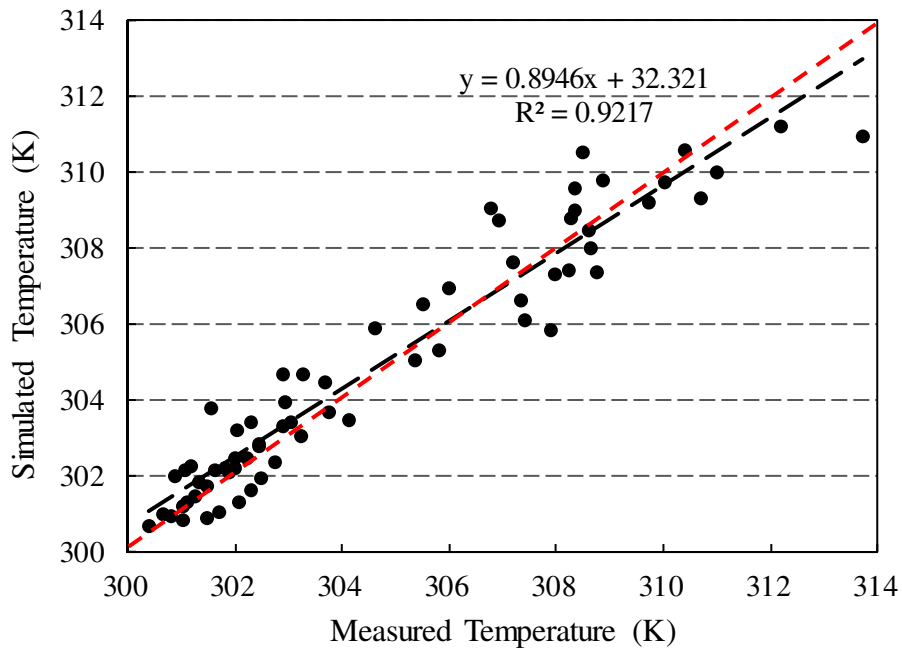
383 3.4 Comparison between the simulation and measurement results

384 Fig. 7 shows the air temperature comparison between the simulated and measured
 385 data for the aspect ratio of 1 ($H/W=1$). The correlation and root mean square error
 386 (RMSE) value for the simulated and measured data are also presented. Simulated air
 387 temperature in the mock-up street canyon showed the same variation trend as the air
 388 temperature measured at the local weather station. The air in the mock-up street
 389 canyon was heated by the surface of the concrete columns and can result in a higher
 390 value than the air temperature at the local weather station sometimes. It could raise
 391 2–6 K at noon. Correlation analysis suggested that the simulated temperatures were in
 392 good agreement with the measured data. Differences between them were generally
 393 within 1 K (the RMSE was 0.0025 for this case), indicating the acceptable accuracy of
 394 the outdoor zonal model. Fig. 8 and Fig. 9 show the air temperature comparisons
 395 between the simulated and measured data for an aspect ratio of 2 and 3, respectively.
 396 Same as the case of moderate aspect ratio, good agreements between the simulated
 397 and measured data were also achieved in the dense and high-density scenarios.



398
399

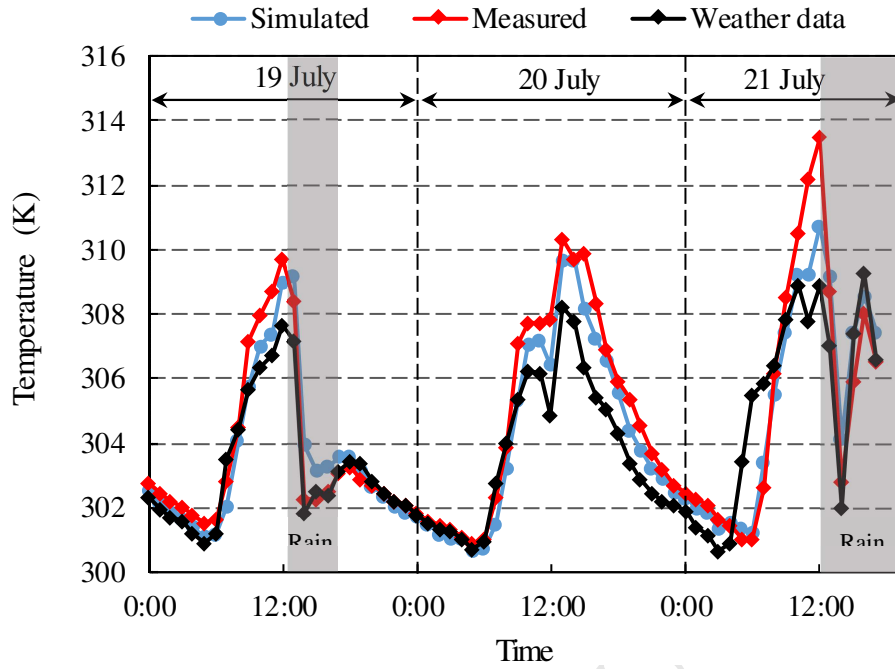
(a)



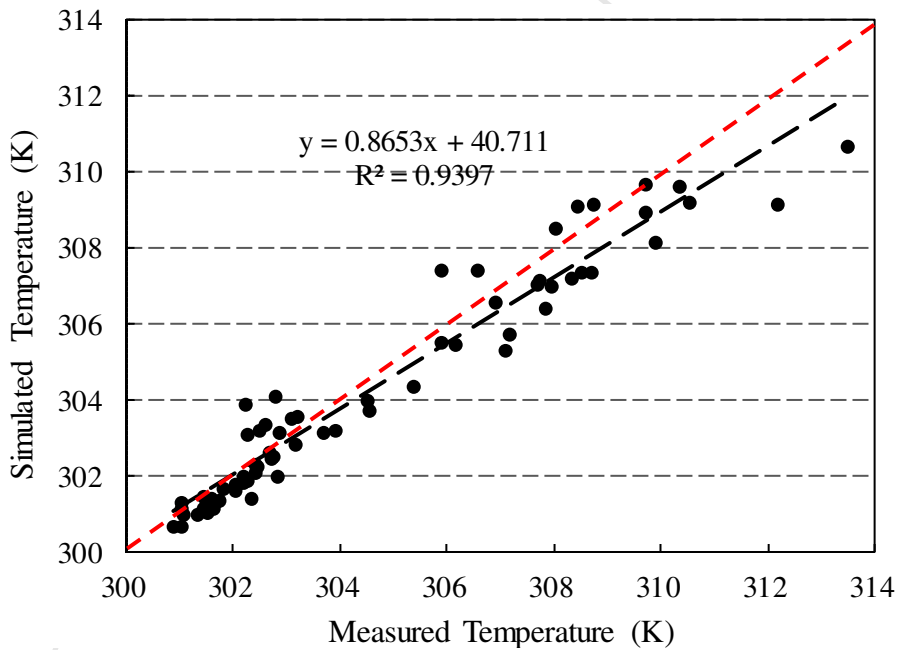
400
401

(b)

402 **Fig. 7** Comparison of the air temperatures in the mock-up street canyon between the
 403 simulated and measured data for the moderate aspect ratio ($H/W=1$). (a) Comparison
 404 between the measured and simulated air temperatures, (b) Correlation analysis
 405 (RMSE=0.0035)

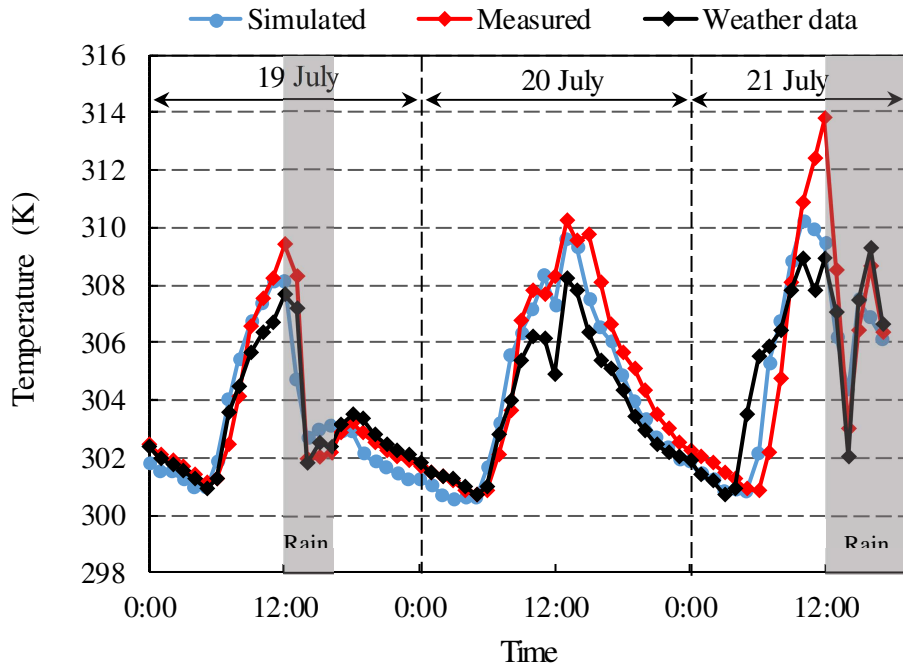


(a)



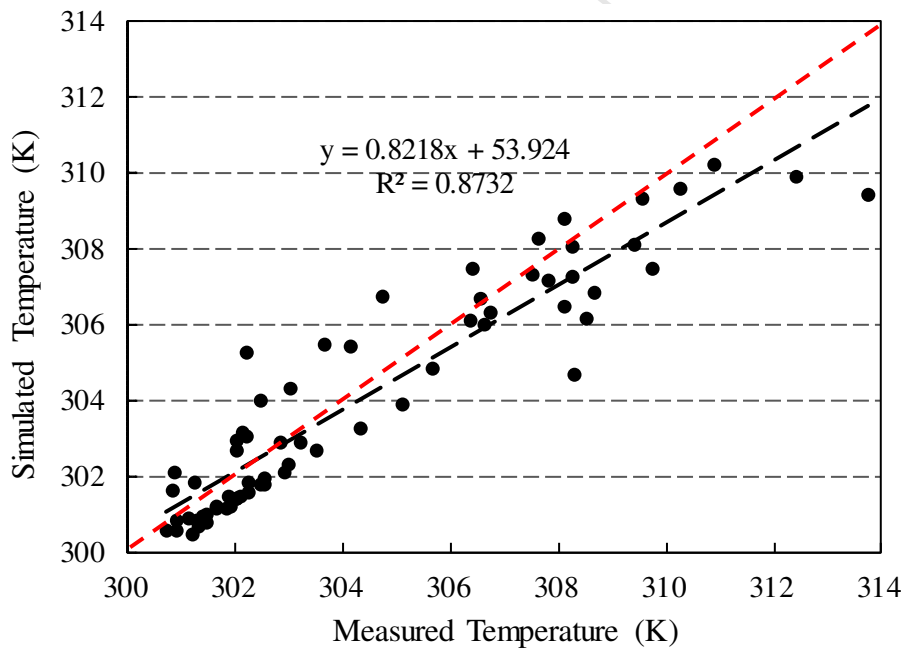
(b)

410 **Fig. 8** Comparison of the air temperatures in the mock-up street canyon between the
 411 simulated and measured data for the dense aspect ratio ($H/W=2$). (a) Comparison
 412 between the measured and simulated air temperatures, (b) Correlation analysis
 413 (RMSE=0.0029)



414
415

(a)



416
417

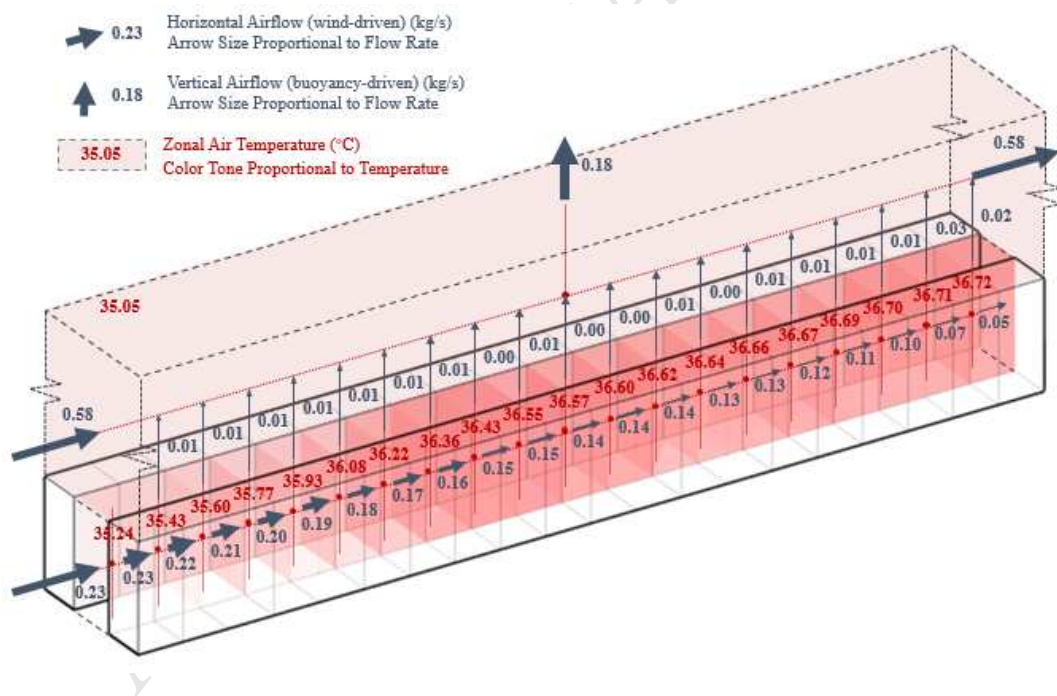
(b)

418 **Fig. 9** Comparison of the air temperatures in the mock-up street canyon between the
 419 simulated and measured data for the high-density aspect ratio ($H/W=3$). (a)
 420 Comparison between the measured and simulated air temperatures, (b) Correlation
 421 analysis (RMSE=0.0041)

422

423 3.5 Strength and limitation of the zonal model

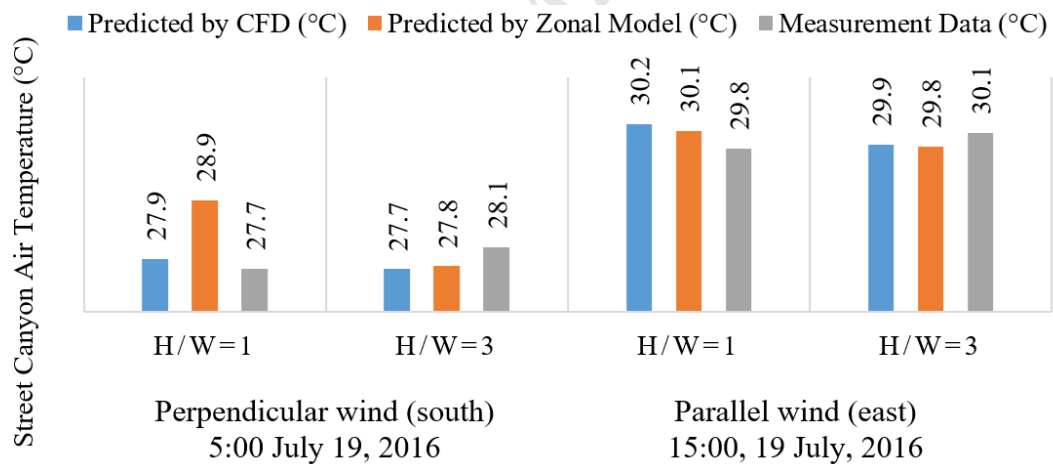
424 The strength of the zonal model lies in its ability to estimate urban buoyancy flow
 425 driven by solar heat gains and anthropogenic heat sources. This model is not intended
 426 to replace CFD modelling; rather, it can serve as a supplement to the existing
 427 state-of-the art methods for rapid calculation over longer time periods, for example,
 428 providing hourly values for a whole year. It is quick and it can be easily coupled with
 429 other simulation platform such as building energy models. Results can be convenient
 430 illustrated for practical applications. The airflow pattern as well as temperature profile
 431 of the street canyon with aspect ratio of 3 at 13:00 Jul.20 are presented in Fig. 10. The
 432 air from the boundary zone came from the west direction, heated by the ground and
 433 vertical surfaces of the mock-up street canyon. Air temperature in the canyon
 434 increased from the west to east consequently.



436 **Fig. 10** Visualization of predicted zonal air temperature and inter-zonal airflow rate in
 437 the mock-up street canyon with aspect ratio of 3 at 13:00 Jul.20, 2016

438

439 The limitation of the zonal model lies in its lack of turbulence model. In order to
 440 examine the impact of turbulence characteristics on canyon temperature, we
 441 conducted CFD simulation of the study site using ANSYS Fluent as well as tracer-gas
 442 experiment. Results show that the zonal model prediction has limitations in the
 443 presence of strong turbulence introduced by perpendicular wind in medium density
 444 urban configuration ($H/W=1$). This effect is more prominent with wind perpendicular
 445 to street canyon consisted of uniform height buildings, where prediction from the
 446 zonal model can be over 1 °C higher than measurement data under our study site
 447 conditions. However, the impact of turbulence is subdued in high-density conditions
 448 (aspect ratio $H/W=3$) or under parallel wind, in which predictions from the zonal
 449 model agree very closely with those from the CFD model and measurement data
 450 (within 0.3 °C). Detailed analysis and discussions are featured in the Supporting
 451 Information.



Time	5:00, 19 July		15:00, 19 July	
Dominant wind direction	Perpendicular wind (south)		Parallel wind (east)	
Aspect ratio	H/W=1	H/W=3	H/W=1	H/W=3
CFD predicted temperature (°C)	27.89	27.72	30.21	29.85
Zonal model predicted temperature (°C)	28.90	27.77	30.08	29.82
Measured air temperature (°C)	27.73	28.09	29.78	30.05

452 Fig. 11 Predicted street canyon air temperature by CFD and zonal model in

453 comparison with measurement data.

454

455 **4. Conclusion**

456 This paper described a zonal model developed to simulate urban microclimate
457 conditions in street canyons. Outdoor field measurements have been carried out for
458 mock-up street canyons constructed from concrete bins including zones with three
459 different aspect ratios ($H/W=1, 2, 3$) on a campus environment to evaluate the model
460 performance. Air temperature in the mock-up street canyons could increase up to 6 K
461 above the ambient conditions at the noon, suggesting the necessity to consider the
462 urban microclimate around the buildings. Predicted air temperatures for the mock-up
463 street canyons showed satisfactory agreement with measurement data (within 1 K) for
464 all three aspect ratio cases. The zonal model can predict in-situ air temperature in
465 high-density cities, and, due to its fast computing speed, can potentially support early
466 stage design. The next step is to couple the zonal model with building energy models
467 to simulate annual hourly solar radiation, surface energy balance, and anthropogenic
468 heat sources for a cluster of buildings in urban context.

469

470 **Acknowledgements**

471 The study is supported by the 33rd Round PDF/RAP Scheme, the Seed Fund for Basic
472 Research (#201509159015) from the University of Hong Kong, the National Natural
473 Science Foundation of China (No 51478486) and the National Science Fund for
474 Distinguished Young Scholars (No 41425020). We appreciate the valuable insight and
475 feedback from Prof. Yuguo Li of the Department of Mechanical Engineering at the
476 University of Hong Kong.

477 **References**

- 478 [1] Y. Zhu, J. Liu, A. Hagishima, J. Tanimoto, Y. Yao, Z. Ma, Evaluation of
479 coupled outdoor and indoor thermal comfort environment and anthropogenic
480 heat, *Build. Environ.* 42 (2007) 1018–1025.
- 481 [2] J. Bouyer, C. Inard, M. Musy, Microclimatic coupling as a solution to improve
482 building energy simulation in an urban context, *Energy Build.* 43 (2011) 1549–
483 1559.
- 484 [3] L. Kamal-chaoui, A. Robert, J.E.L.C. Q, Competitive cities and climate change,
485 *Cities.* (2009) 172.
- 486 [4] A.G. Aguilár, P.M. Ward, Globalization, regional development, and mega-city
487 expansion in Latin America: Analyzing Mexico city's peri-urban hinterland,
488 *Cities.* 20 (2003) 3–21.
- 489 [5] E. Ng, Towards planning and practical understanding of the need for
490 meteorological and climatic information in the design of high-density cities: A
491 case-based study of Hong Kong, *Int. J. Climatol.* 32 (2012) 582–598.
- 492 [6] A.M. Rizwan, L.Y.C. Dennis, C. Liu, A review on the generation,
493 determination and mitigation of Urban Heat Island, *J. Environ. Sci.* 20 (2008)
494 120–128.
- 495 [7] T.R. Oke, City Size and the Urban Heat Island, *Atmos. Environ.* 7 (1973) 769–
496 779.
- 497 [8] J. Yang, Z.H. Wang, K.E. Kaloush, H. Dylla, Effect of pavement thermal
498 properties on mitigating urban heat islands: A multi-scale modeling case study
499 in Phoenix, *Build. Environ.* 108 (2016) 110–121.
- 500 [9] A. Gros, E. Bozonnet, C. Inard, Cool materials impact at district scale -
501 Coupling building energy and microclimate models, *Sustain. Cities Soc.* 13
502 (2014) 254–266.
- 503 [10] E. Erell, T. Williamson, Comments on the correct specification of the
504 analytical CTTC model for predicting the urban canopy layer temperature,
505 *Energy Build.* 38 (2006) 1015–1021.
- 506 [11] M. Santamouris, N. Papanikolaou, I. Koronakis, I. Livada, D. Asimakopoulos,
507 Thermal and air flow characteristics in a deep pedestrian canyon under hot
508 weather conditions, *Atmos. Environ.* 33 (1999) 4503–4521.
- 509 [12] E. Johansson, Influence of urban geometry on outdoor thermal comfort in a hot
510 dry climate: A study in Fez, Morocco, *Build. Environ.* 41 (2006) 1326–1338.
- 511 [13] S. Karra, L. Malki-Epshtein, M.K.A. Neophytou, Air flow and pollution in a

- 512 real, heterogeneous urban street canyon: A field and laboratory study, *Atmos.*
513 *Environ.* 165 (2017) 370–384.
- 514 [14] M. Bruse, H. Fleer, Simulating surface-plant-air interactions inside urban
515 environments with a three dimensional numerical model, *Environ. Model.*
516 *Softw.* 13 (1998) 373–384.
- 517 [15] A. Chatzidimitriou, K. Axarli, Street canyon geometry effects on microclimate
518 and comfort; A case study in Thessaloniki, *Procedia Environ. Sci.* 38 (2017)
519 643–650.
- 520 [16] M. Oguro, Y. Morikawa, S. Murakami, K. Matsunawa, A. Mochida, H.
521 Hayashi, Development of a wind environment database in Tokyo for a
522 comprehensive assessment system for heat island relaxation measures, *J. Wind*
523 *Eng. Ind. Aerodyn.* 96 (2008) 1591–1602.
- 524 [17] X. Yang, Y. Li, The impact of building density and building height
525 heterogeneity on average urban albedo and street surface temperature, *Build.*
526 *Environ.* 90 (2015) 146–156.
- 527 [18] X. Li, Z. Yu, B. Zhao, Y. Li, Numerical analysis of outdoor thermal
528 environment around buildings, *Build. Environ.* 40 (2005) 853–866.
- 529 [19] B. Lin, X. Li, Y. Zhu, Y. Qin, Numerical simulation studies of the different
530 vegetation patterns' effects on outdoor pedestrian thermal comfort, *J. Wind*
531 *Eng. Ind. Aerodyn.* 96 (2008) 1707–1718.
- 532 [20] R. Yao, Q. Luo, B. Li, A simplified mathematical model for urban
533 microclimate simulation, *Build. Environ.* 46 (2011) 253–265.
- 534 [21] S. Gracik, M. Heidarinejad, J. Liu, J. Srebric, Effect of urban neighborhoods on
535 the performance of building cooling systems, *Build. Environ.* 90 (2015) 15–29.
- 536 [22] A. Jeanjean, R. Buccolieri, J. Eddy, P. Monks, R. Leigh, Air quality affected by
537 trees in real street canyons: The case of Marylebone neighbourhood in central
538 London, *Urban For. Urban Green.* 22 (2017) 41–53.
- 539 [23] C.Y. Wen, Y.H. Juan, A.S. Yang, Enhancement of city breathability with half
540 open spaces in ideal urban street canyons, *Build. Environ.* 112 (2017) 322–336.
- 541 [24] Z.T. Ai, C.M. Mak, CFD simulation of flow in a long street canyon under a
542 perpendicular wind direction: Evaluation of three computational settings, *Build.*
543 *Environ.* 114 (2017) 293–306.
- 544 [25] X. Jin, L. Yang, X. Du, Y. Yang, Transport characteristics of PM_{2.5} inside
545 urban street canyons: The effects of trees and vehicles, *Build. Simul.* 10 (2017)
546 1–14.
- 547 [26] M. Moradpour, H. Afshin, B. Farhanieh, A numerical study of reactive

- 548 pollutant dispersion in street canyons with green roofs, *Build. Simul.* (2017).
- 549 [27] L. Yang, Y. Li, Thermal conditions and ventilation in an ideal city model of
550 Hong Kong, in: *Energy Build.*, 2011: pp. 1139–1148.
- 551 [28] F.S. De La Flor, S.A. Domínguez, Modelling microclimate in urban
552 environments and assessing its influence on the performance of surrounding
553 buildings, in: *Energy Build.*, 2004: pp. 403–413.
- 554 [29] M. Musy, E. Wurtz, F. Winkelmann, F. Allard, Generation of a zonal model to
555 simulate natural convection in a room with a radiative/convective heater, *Build.*
556 *Environ.* 36 (2001) 589–596.
- 557 [30] E. Bozonnet, R. Belarbi, F. Allard, Modelling air flows around buildings in
558 urban environment, *Int. Work. Energy Perform. Environ. Qual. Build.* (2006)
559 1–6.
- 560 [31] R. Djedjig, E. Bozonnet, R. Belarbi, Modeling green wall interactions with
561 street canyons for building energy simulation in urban context, *Urban Clim.* 16
562 (2016) 75–85.
- 563 [32] V. Masson, A physically-based scheme for the urban energy budget in
564 atmospheric models, *Boundary-Layer Meteorol.* 94 (2000) 357–397.
- 565 [33] C. Inard, H. Bouia, P. Dalicieux, Prediction of air temperature distribution in
566 buildings with a zonal model, *Energy Build.* 24 (1996) 125–132.
- 567 [34] A.C. Megri, F. Haghighat, Zonal Modeling for Simulating Indoor Environment
568 of Buildings: Review, Recent Developments, and Applications, *HVAC&R Res.*
569 13 (2007) 887–905.
- 570 [35] C.R. Chu, Y.H. Chiu, Y.J. Chen, Y.W. Wang, C.P. Chou, Turbulence effects
571 on the discharge coefficient and mean flow rate of wind-driven
572 cross-ventilation, *Build. Environ.* 44 (2009) 2064–2072.
- 573 [36] Y. Li, A. Delsante, J. Symons, Prediction of natural ventilation in buildings
574 with large openings, *Build. Environ.* 35 (2000) 191–206.
- 575 [37] S.W. Dols, G.N. Walton, *CONTAMW 2.0 User Manual*, U.S. Dep. Commer.
576 (2002).
- 577 [38] C. Chang, R.N. Meroney, Numerical and physical modeling of bluff body flow
578 and dispersion in urban street canyons, *J. Wind Eng. Ind. Aerodyn.* (2001) 1–8.
- 579 [39] J.S. Irwin, A theoretical variation of the wind profile power-law exponent as a
580 function of surface roughness and stability, *Atmos. Environ.* 13 (1979) 191–
581 194.
- 582 [40] A. Albani, M.Z. Ibrahim, Wind energy potential and power law indexes

- 583 assessment for selected near-coastal sites in Malaysia, *Energies*. 10 (2017) 1–
584 21.
- 585 [41] W. Theurer, W. Baechlin, E.J. Plate, Model study of the development of
586 boundary layers above urban areas, *J. Wind Eng. Ind. Aerodyn.* 41 (1992) 437–
587 448.
- 588 [42] P.A. Favarolo, H. Manz, Temperature-driven single-sided ventilation through a
589 large rectangular opening, *Build. Environ.* 40 (2005) 689–699.
- 590 [43] D. Etheridge, *Natural ventilation of buildings: theory, measurement and design*,
591 2011.

Figure captions

Fig. 1 Schematic depiction of the zonal urban microclimate model. (The solid blocks describe the buildings)

Fig. 2 The experiment site. (a) Schematic illustration of the plan of the mock-up street canyons with aspect ratios of moderate ($H/W=1$), dense ($H/W=2$), and high-density ($H/W=3$), (b) Aerial photo of the mock-up site taken on 18 July 2016, (c) Horizontal photos of the mock-up site taken on 18 July 2016

Fig. 3 Instrument layout in the mock-up street canyon. (a) Illustration of the locations of the instruments (the “○” represents the thermocouples), (b) Photo of the sensors

Fig. 4 Boundary conditions measured by the local weather station during the measurement. (a) Air temperature and barometric pressure, (b) Wind speed and direction

Fig. 5 Division of zones for the mock-up street canyon

Fig. 12 Convergence of pressure, temperature and air flow at a typical hour. (a) Pressure residual, (b) Temperature residual, (a) Airflow residual

Fig. 7 Comparison of the air temperatures in the mock-up street canyon between the simulated and measured data for the moderate aspect ratio ($H/W=1$). (a) Comparison between the measured and simulated air temperatures, (b) Correlation analysis (RMSE=0.0025)

Fig. 8 Comparison of the air temperatures in the mock-up street canyon between the simulated and measured data for the dense aspect ratio ($H/W=2$). (a) Comparison between the measured and simulated air temperatures, (b) Correlation analysis (RMSE=0.0029)

Fig. 9 Comparison of the air temperatures in the mock-up street canyon between the

simulated and measured data for the high-density aspect ratio ($H/W=3$). (a) Comparison between the measured and simulated air temperatures, (b) Correlation analysis (RMSE=0.0041)

Fig. 10 Visualization of predicted zonal air temperature and inter-zonal airflow rate in the mock-up street canyon with aspect ratio of 3 at 13:00 Jul.20, 2016

Research Highlights

- Developed a zonal model to assess street canyon air temperature of high-density cities
- The model was evaluated in field measurement on a mock-up site with 3 aspect ratios
- Good agreements between predicted and measured air temperatures were observed (<1 K)
- Peak warming between 2-6 K above the ambient air temperature were observed in mockup street canyons